

Mechanisms of Transport in Radiative Improved Mode

TOKAR M.Z., DUMORTIER P.¹, JACKSON G.L.², KALUPIN D.¹, MURAKAMI M.^{2,3},
MESSIAEN A.M.¹, NORDMAN H.⁴, ONGENA J.¹, REISER D., SINGH R.⁵, STAEBLER G.M.²,
SYDORA R.⁶, UNTERBERG B., WEILAND J.⁴ and WEYNANTS R.R.¹

Institut für Plasmaphysik, Association EURATOM-FZJ, 52425, Jülich, Germany

¹*ERM-KMS, Association „EURATOM-Belgian State“, Brussels, Belgium*

²*DIII-D National Fusion Facility, San Diego, CA 92 186-5698, USA*

³*ORNL, Oak Ridge, TN 3783 1-8072, USA*

⁴*Chalmers University of Technology, Association EURATOM-NFR, Göteborg, Sweden*

⁵*Institute for Plasma Research, Bhat, Gandhinagar, India*

⁶*University of Alberta, Edmonton, Alberta, Canada T6G 2J1*

(Received: 11 December 2001 / Accepted: 20 March 2002)

Abstract

Improvement of confinement by a deliberate seeding of impurities like neon and argon has been found in many devices. Most intensively this phenomenon was studied in the limiter tokamak TEXTOR, where it was called radiative improved (RI) mode, and in the divertor machine DIII-D. Recent experiments on TFTR, JT-60 and JET have demonstrated that by an optimization of seeding procedure a positive effect of impurities can be achieved in reactor scale devices.

Extensive theoretical and modelling activities were performed during past years in order to understand the mechanisms of confinement improvement in RI-mode. Characteristics of drift instabilities namely the ion temperature gradient (ITG) and dissipate trapped electron (DTE) modes, which provide the main contribution to the anomalous transport in tokamaks, have been analyzed by the code for Gyro-Kinetic Stability. The behavior of non-linear turbulent eddies and vortices was studied in “particle in cell” simulations. Fluid approximation has been applied to assess the effect of impurities on anomalous transport. All these studies predict a reduction of turbulence originated from the most dangerous ITG modes. Computations by a transport code with models for anomalous transport coefficients due to drift micro-instabilities reproduce many peculiarities of RI-plasmas.

Keywords:

drift instability, confinement improvement, impurity, turbulence suppression

1. Introduction

Operational regimes with reduced anomalous transport resulting from seeding of impurities were obtained in different tokamaks, e.g., in ISX-B, ASDEX, TEXTOR, DIII-D, TFTR [1]. In these experiments a deliberate pollution of the plasma led to an improvement of the energy confinement in spite of increased radiation losses. Understanding of mechanisms, which underlie

such a surprising effect of impurities on plasma performance, is important to assess the relevance of these regimes to reactor conditions.

2. Features of L-RI Transition

In the limiter tokamak TEXTOR the transition to radiative improved (RI) mode from a state of low (L)

Corresponding author's e-mail: m.tokar@fz-juelich.de

©2002 by The Japan Society of Plasma
Science and Nuclear Fusion Research

confinement was triggered by puffing of neon impurity in plasmas additionally heated by neutral beam injection (NBI) and ion cyclotron resonance heating (ICRH). As an example Fig.1 displays the measured radial profiles of the electron and ion temperatures and electron density

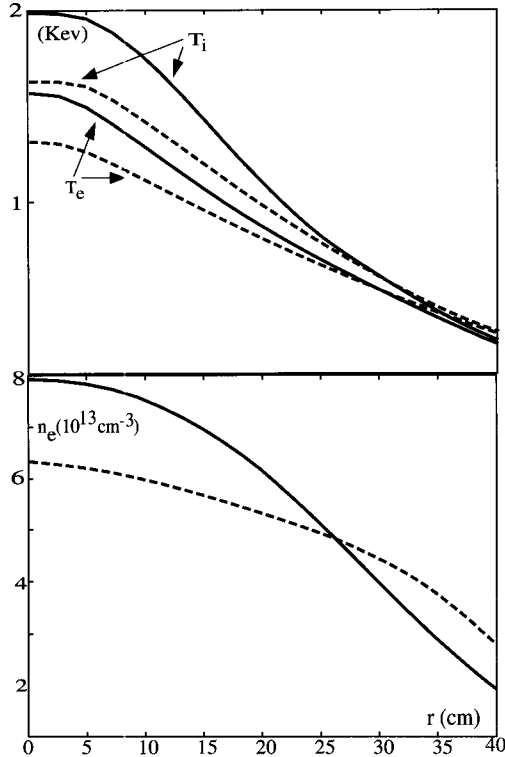


Fig. 1 Radial profiles of plasma parameters in shot 68803 in TEXTOR measured in L-mode before neon puff (broken curves) and in RI-mode (solid lines).

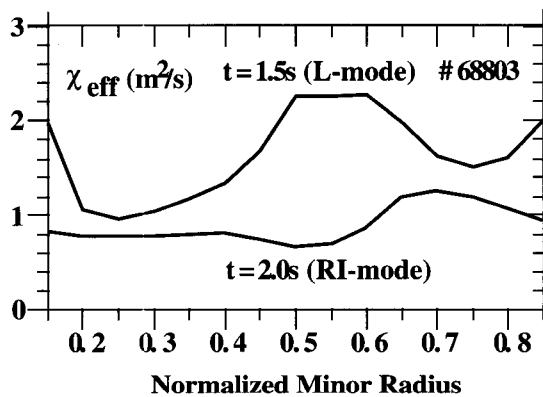


Fig. 2 Radial profiles of effective heat diffusivity found in TRANSP analysis.

in the L-mode and RI-mode stages in shot 68803 [2]. Although all profiles are more peaked in the RI-mode the most pronounced feature is the principal change in the density shape. In Fig. 2 the reduction of anomalous transport is demonstrated by the radial profiles of the effective heat diffusivity obtained from TRANSP modeling [2].

3. Changes in Transport Characteristics

The analysis of drift mode stability by different approaches shows that the observed reduction in anomalous transport in the RI-mode is caused by a significant suppression of Ion Temperature Gradient (ITG) unstable modes. These modes are widely considered as the main cause of anomalous losses of energy and particles in the L-mode. Figure 3 shows the perpendicular wave number spectrum of the ITG growth rate γ_{ITG} found in ref. [3] on the bases of a fluid model [4] generalized for the case of arbitrary number of ion species.

In order to understand the reasons for the decrease of γ_{ITG} in RI-mode we proceed from an approximate formula derived for plasmas with a not very flat density profile [5]:

$$\gamma_{ITG}^{max} \propto \sqrt{\frac{-\frac{d \ln T_i}{dr} + \frac{2}{3} \frac{d \ln n_e}{dr}}{Z_{eff}} - \frac{R}{8} \left(\frac{d \ln n_e}{dr} \right)^2}$$

The plasma effective charge Z_{eff} comes into play because the trigger of ITG instability, non divergence free due to tokamak geometry diamagnetic flow, is inversely

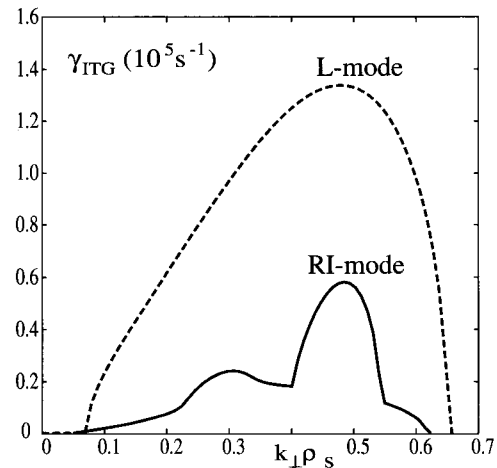


Fig. 3 Spectrum of the ITG instability growth rate at $r=30$ cm under L- and RI-mode conditions in TEXTOR.

proportional to the ion charge. There are two channels for the influence of the density gradient: (i) the work of pressure gradient and (ii) phase shift between the density and temperature perturbations. One can see that only an increase in Z_{eff} is not enough to suppress the instability and a simultaneous increase of the density gradient, i.e., density peaking is required.



Fig. 4 The pattern of the electrostatic potential in the poloidal cross-section found by "particle in cell" modelling of drift turbulence in L- (left) and RI-mode (right).

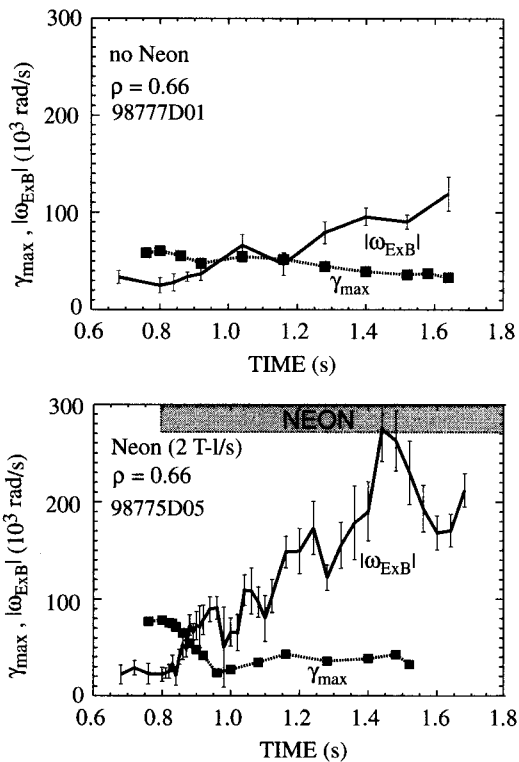


Fig. 5 Time evolution of the maximum growth rate and shear of $E \times B$ rotation in DIII-D L-mode discharges without and with neon seeding.

The results of simple stability analysis agree with the data of sophisticated modelling by the "particle in cell" approach [6]. Figure 4 demonstrates the modification in the poloidal distribution of the electrostatic potential occurred by the L-RI transition. After the transition the turbulence is strongly reduced in the main part of the plasma cross-section and this is mostly due to the more peaked density profile in the RI-mode.

It is necessary to stress that the discussed mechanisms of turbulence suppression in RI-mode do not rely on the traditional scenario due to a sheared radial electric field E_r . However the latter can be of significant importance in discharges with unbalanced NBI injection where a strong toroidal rotation contributes essentially to E_r . Figure 5 shows the time evolution of the maximum growth rate of drift modes and the radial shear of $E \times B$ rotation in two shots in DIII-D [7]. Neon injection triggers the process of continuous rise in the $|\omega_{ExB}|$. This happens, however, after the initial drop in the maximum growth rate due to the presence of impurities [7]. The turbulence becomes completely suppressed when $\gamma_{\text{max}} < |\omega_{ExB}|$. In discharges with balanced NBI $|\omega_{ExB}|$ does play an essential role and only direct effect of impurities leads to confinement improvement.

4. Role and Mechanism of Density Peaking

Observations on TEXTOR show that density peaking is indeed an important prerequisite of the L-RI transition [8]. In Fig. 6 the improvement factor f_{H93} is

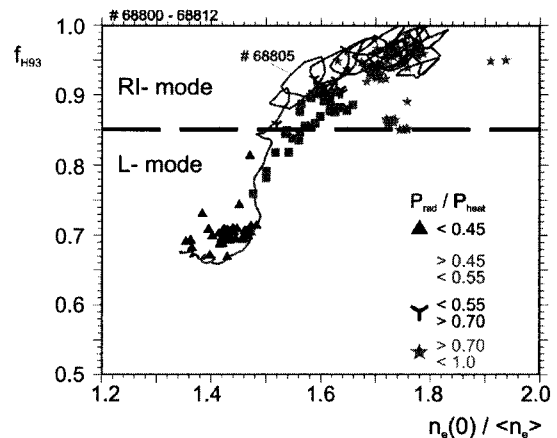


Fig. 6 Improvement factor f_{H93} versus density peaking for discharges with different radiation level. The curve shows the time evolution of both parameters in TEXTOR shot 68805.

displayed as a function of the ratio between the central and line averaged values of the density. A certain critical level of peaking should be achieved before the transition. In order to get an idea what is the cause of the peaking we proceed from an electron particle balance equation. For stationary conditions in the plasma core where particle sources are weak this condition reduces to zero flux density:

$$\Gamma_{\perp}^e \equiv -D_{\perp}^e \frac{\partial n_e}{\partial r} + V_{\perp}^e n_e \approx 0$$

Thus a peaking of the density profiles should occur due to increase in the ratio of pinch velocity V_{\perp}^e and diffusivity D_{\perp}^e . An interpretive analysis has shown [9]

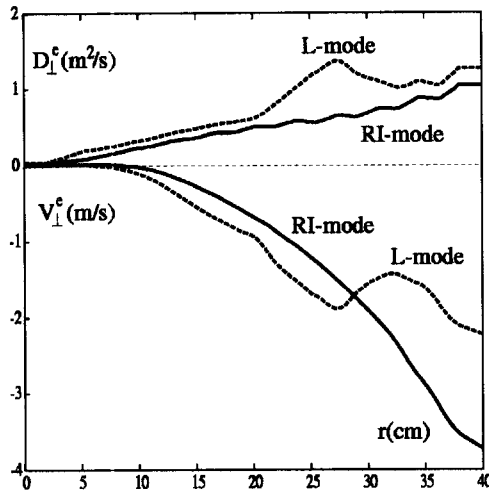


Fig. 7 Electron diffusivity and pinch velocity reconstructed by an interpretive analysis for L- and RI-mode conditions in TEXTOR.

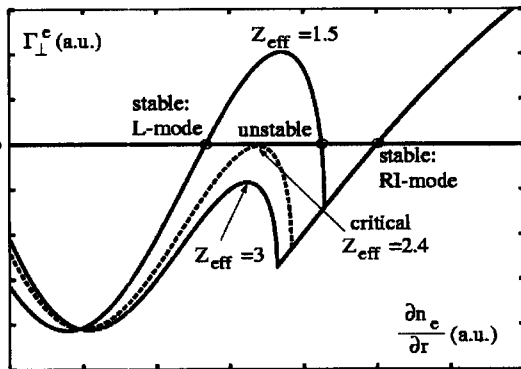


Fig. 8 Dependencies of the electron flux density on the density gradient and stationary plasma states for different conditions.

that this happens mainly because of reduction in the particle diffusivity (see Fig. 7).

5. Predictive Transport Modeling

5.1 Transport model for L-RI bifurcation

In the literature one can find theoretical approaches, which allow to interpret the modification in transport characteristics observed by the L-RI transition [10,11]. When the anomalous transport is due to instabilities on ion dynamics, e.g. ITG, the relative level of pinch-velocity is small. In the case with turbulence dominated by trapped electrons (TE) this level is significantly larger. The following half-empirical transport model takes this into account:

$$D_{\perp}^e = D_{\perp}^{ITG} + D_{\perp}^{DTE}, \quad V_{\perp}^e = - \left(D_{\perp}^{ITG} \frac{4r}{3R} + D_{\perp}^{DTE} \right) \frac{d \ln q}{dr}$$

where the q is the safety factor and the diffusivity ingredients due to different unstable modes are computed in the mixing length limit:

$$D_{\perp}^{ITG, DTE} \propto \gamma_{ITG, DTE}^{\max} / k_{\perp, \max}^2$$

with $k_{\perp, \max}$ being the perpendicular wave number at which the growth rates achieves its maximum (γ_{DTE} is computed according to Ref. [12]).

Figure 8 displays the electron flux density Γ_{\perp}^e versus the density gradient for parameters at $r=30\text{cm}$ in TEXTOR in L-, RI-mode and under some intermediate critical conditions. In the L-mode with a low plasma effective charge 3 stationary values of dn_e/dr are possible. The discharge history predetermines that the plasma is in the stable state of a low gradient. An increase of Z_{eff} results in the reduction of the ITG contribution and Γ_{\perp}^e maximum decreases. When the critical state is reached a dynamic bifurcation to the RI-mode state with a large density gradient occurs.

5.2 Numerical predictive modelling by code RITM

TEXTOR: The transport model described above has been incorporated into 1-D transport code RITM [13] developed especially to model the plasma states strongly influenced by impurities through radiation, ion dilution and, now, effects on transport coefficients. RITM describes the transport of hydrogen and impurity neutrals and allows to model the role of recycling. The sources due to ionization of neutrals are included into continuity equations for electrons and all charge states of such impurities as He, C, O, Ne, Si. Heat balance equations for

electrons and ions are solved with the energy sources from ohmic, NBI and ICR heating. The profile of ohmic current is computed from Maxwell equations and Grad-Shafranov equation determines the shift of magnetic surfaces. Together with analytically prescribed profiles of ellipticity and triangularity this allows to calculate the metric coefficients.

Figure 9 demonstrates the time evolution of the density profile modeled with RITM for a discharge where seeding of neon leads to the L-RI transition. Starting from some initial profiles the prescribed program for the line averaged density is controlled by the gas puff intensity. To a time of 0.12s a centrally flat

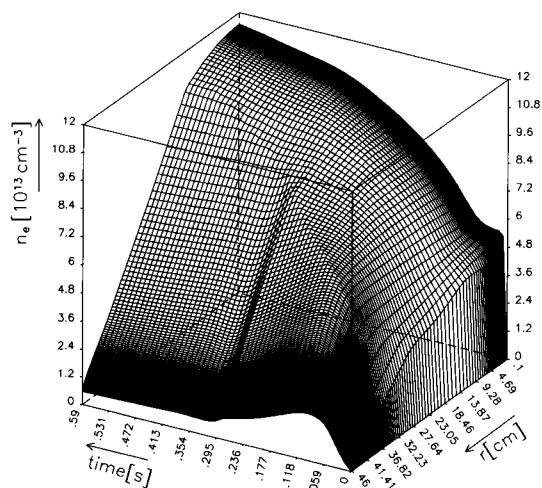


Fig. 9 Modeled by the code RITM time evolution of the electron density profile during the L-RI transition by neon puffing into TEXTOR.

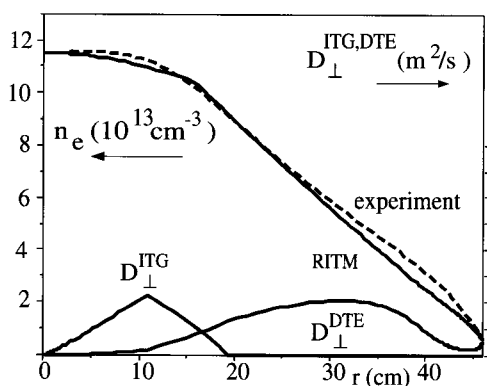


Fig. 10 Final density profile after the L-RI transition in TEXTOR measured (broken line) and computed by RITM with contributions of different channels to anomalous particle diffusion (solid lines).

profile typical for L-mode is formed. Later the presence of impurity leads to a subsequent penetration of the L-RI bifurcation towards the plasma core. At a time of 0.3 s quasi-stationary RI-mode conditions are reached, which are characterized by a peaked density profile, a high radiation fraction $P_{rad}/P_{tot} \sim 0.7$ and ITG mode suppressed over a wide radial zone of the plasma. From this moment the intensity of gas puff is fixed at a very low level. Nevertheless the density profile continues to peak and the central electron density exceeds $1.1 \times 10^{14} \text{ cm}^{-3}$ (see Fig. 10).

JET: Earlier trials to improve confinement in JET by seeding of impurities [14] sowed doubts that this can be achieved in large machines. New series of experiments have shown that also in this case a positive effect of impurity seeding can be attained through an optimization of the puffing scenario both for the working and impurity gases. It was possible, e.g., to maintain a good confinement in the H-mode discharges at an electron density close to the Greenwald limit. In the L-mode discharges seeding of neon led as in TEXTOR and DIII-D to a significant, however transient, peaking of density and pressure. Figures 11 and 12 show the measured and computed by RITM, resp., profiles of plasma parameters in #50329 before and after neon puff. The modeling allowed to interpret the necessity of a significantly higher plasma effective charge in JET, 5-7, than in DIII-D and TEXTOR, 2-3, in order to get an RI-mode effect. The

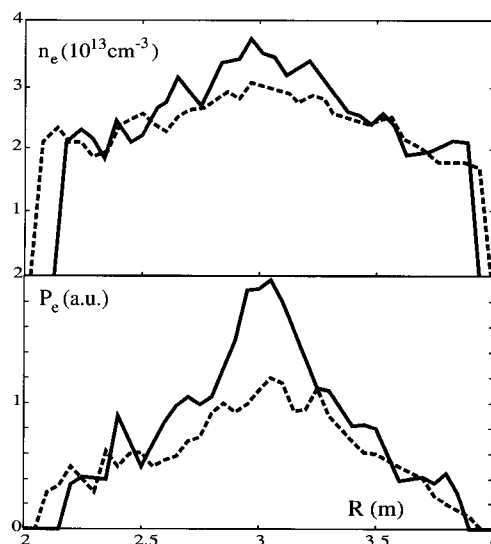


Fig. 11 Electron density and pressure profiles in JET #50329: L-mode (broken curves) before and RI-mode like state (solid curves) after neon seeding.

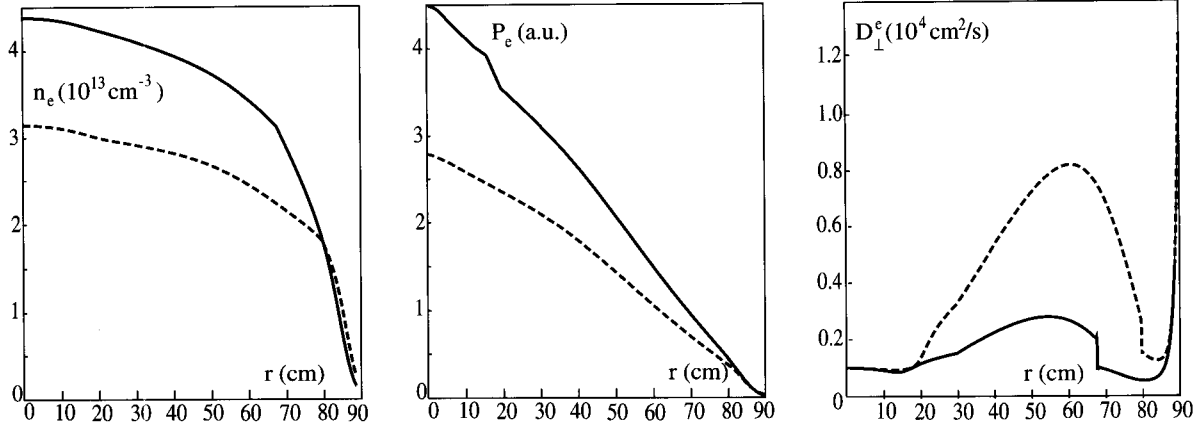


Fig. 12 Computed profiles of the electron density, pressure and diffusivity for JET shot # 50329: L-mode (broken curves) before and RI-mode like state (solid curves) after neon seeding.

ratio V_{\perp}^c/D_{\perp}^c , which controls the density peaking, is governed by the value $D_{\perp}^{\text{DTE}}/D_{\perp}^{\text{ITG}}$ and for a bifurcation to the RI-mode the latter should exceed a critical level [5]. On the one hand in plasmas of low collisionality as in JET, the electron drift frequency exceeds the effective collision frequency for trapped electrons and $D_{\perp}^{\text{DTE}} \sim n_e$ [12]. On the other hand D_{\perp}^{ITG} decreases with increasing Z_{eff} and ITG transport is suppressed completely when the plasma effective charge exceeds a certain critical level [5]. Thus the lower the plasma density the higher Z_{eff} , at which $D_{\perp}^{\text{DTE}}/D_{\perp}^{\text{ITG}}$ approaches its critical level. Since the plasma in JET L-mode is hotter and of a lower density than in DIII-D and TEXTOR the required Z_{eff} is larger.

6. Conclusion

Radiative improved mode was found in diverse tokamaks by seeding of different impurities. It is accompanied by a significant reduction in the anomalous transport of energy and particles. Both simple transport models and sophisticated simulations confirm that this happens due to suppression of ITG turbulence which is the main transport channel in L-mode. The suppression is initiated by the increase of Z_{eff} and enhanced by peaking of the density profile occurred due to increase of the V_{\perp}^c/D_{\perp}^c ratio. At a high enough Z_{eff} a bifurcation leading to the L-RI transition takes place. In computations with the code RITM the transport

models with contribution from ITG and TE modes to the particle flux reproduces well the profile evolution in TEXTOR and JET caused by impurity seeding.

References

- [1] J. Ongena *et al.*, *Phys. Plasmas* **8**, 2188 [2001].
- [2] R.R. Weynants *et al.*, *Nucl. Fusion* **39**, 1637 [1999].
- [3] M.Z. Tokar' *et al.*, *Plasma Phys. Control. Fusion* **41**, L9 [1999].
- [4] J. Weiland *Collective Modes in Inhomogeneous Plasmas, Kinetic and Advanced Fluid Theory* (Bristol: IOP Publishing, 2000).
- [5] M.Z. Tokar *et al.*, *Phys. Rev. Lett.* **84**, 895 [2000].
- [6] R. Sydora *et al.*, *Plasma Phys. Control. Fusion* **38**, A281 [1996].
- [7] G.R. McKee *et al.*, *Phys. Plasmas* **7**, 1870 [2000].
- [8] B. Unterberg *et al.*, *Plasma Phys. Control. Fusion* **39**, B189 [1997].
- [9] M.Z. Tokar, *Contrib. Plasma Phys.* **40**, 443 [2000].
- [10] V.V. Yankov and J. Nycander, *Phys. Plasmas* **4**, 2907 [1997].
- [11] D.R. Baker and M.N. Rosenbluth, *Phys. Plasmas* **5**, 2936 [1998].
- [12] B.B. Kadomtsev and O.P. Pogutse, *Nucl. Fusion* **11**, 67 [1971].
- [13] M.Z. Tokar, *Plasma Phys. Control. Fusion* **36**, 1819 [1994].
- [14] G.F. Matthews *et al.*, *Nucl. Fusion* **39**, 19 [1999].